AMERICAN SOCIETY FOR MICROBIOLOGY | Antimicrobial Agents and Chemotherapy®

EXPERIMENTAL THERAPEUTICS

The Added Value of Longitudinal Imaging for Preclinical *In Vivo* Efficacy Testing of Therapeutic Compounds against Cerebral Cryptococcosis

Liesbeth Vanherp,[a,b] Jennifer Poelmans,[a,b]* Amy Hillen,[a,b]* Guilhem Janbon,[c] Matthias Brock,[d] Katrien Lagrou,[e,f] Greetje Vande Velde,[a,b] Uwe Himmelreich[a,b]

[a]Biomedical MRI, Department of Imaging and Pathology, KU Leuven, Leuven, Belgium
[b]Molecular Small Animal Imaging Center, KU Leuven, Leuven, Belgium
[c]RNA Biology of Fungal Pathogens, Department of Mycology, Pasteur Institute, Paris, France
[d]Fungal Biology Group, School of Life Sciences, University of Nottingham, Nottingham, United Kingdom
[e]Laboratory of Clinical Bacteriology and Mycology, Department of Microbiology, Immunology and Transplantation, KU Leuven, Leuven, Belgium
[f]National Reference Centre for Mycosis, Department of Laboratory Medicine, University Hospitals Leuven, Leuven, Belgium

Greetje Vande Velde and Uwe Himmelreich contributed equally to this article.

ABSTRACT Brain infections with *Cryptococcus neoformans* are associated with significant morbidity and mortality. Cryptococcosis typically presents as meningoencephalitis or fungal mass lesions called cryptococcomas. Despite frequent *in vitro* discoveries of promising novel antifungals, the clinical need for drugs that can more efficiently treat these brain infections remains. A crucial step in drug development is the evaluation of *in vivo* drug efficacy in animal models. This mainly relies on survival studies or postmortem analyses in large groups of animals, but these techniques only provide information on specific organs of interest at predefined time points. In this proof-of-concept study, we validated the use of noninvasive preclinical imaging to obtain longitudinal information on the therapeutic efficacy of amphotericin B or fluconazole monotherapy in meningoencephalitis and cryptococcoma mouse models. Bioluminescence imaging enabled the rapid *in vitro* and *in vivo* evaluation of drug efficacy, while complementary high-resolution anatomical information obtained by magnetic resonance imaging of the brain allowed a precise assessment of the extent of infection and lesion growth rates. We demonstrated a good correlation between both imaging readouts and the fungal burden in various organs. Moreover, we identified potential pitfalls associated with the interpretation of therapeutic efficacy based solely on postmortem studies, demonstrating the added value of this noninvasive dual imaging approach compared to standard mortality curves or fungal load endpoints. This novel preclinical imaging platform provides insights in the dynamic aspects of the therapeutic response and facilitates a more efficient and accurate translation of promising antifungal compounds from bench to bedside.

KEYWORDS animal models, antifungal therapy, bioluminescence imaging, central nervous system infections, cryptococcosis, *in vivo*, magnetic resonance imaging, noninvasive imaging

Fungal infections of the central nervous system (CNS) are generally associated with high mortality rates and poor prognosis (1). The group of patients at risk for contracting these opportunistic infections has grown due to the increased prevalence of disease-induced or treatment-related immunosuppression (2). Of the few fungal species able to infect the brain, *Cryptococcus neoformans* is worldwide one of the most common causative organisms (2). It infects mainly HIV patients but also persons with

Citation Vanherp L, Poelmans J, Hillen A, Janbon G, Brock M, Lagrou K, Vande Velde G, Himmelreich U. 2020. The added value of longitudinal imaging for preclinical *in vivo* efficacy testing of therapeutic compounds against cerebral cryptococcosis. Antimicrob Agents Chemother 64:e00070-20. https://doi.org/10.1128/AAC.00070-20.

Address correspondence to Greetje Vande Velde, greetje.vandevelde@kuleuven.be.

* Present address: Jennifer Poelmans, The Janssen Pharmaceutical Companies of Johnson & Johnson, Beerse, Belgium; Amy Hillen, Department of Cell and Molecular Biology, Karolinska Institutet, Stockholm, Sweden.

Received 13 January 2020
Returned for modification 22 March 2020
Accepted 4 April 2020
Accepted manuscript posted online 13 April 2020
Published 23 June 2020

underlying medical conditions or receiving immunosuppressive treatment and, occasionally, immunocompetent individuals (3). Cryptococcal infection of the CNS arises after dissemination or reactivation of fungal cells that were initially acquired through inhalation. Most frequently, the disease presents as a subacute meningoencephalitis, with small accumulations of yeasts in the brain parenchyma (4, 5). More rarely, it causes mass lesions in the brain parenchyma, called cryptococcomas (1). These occur more frequently in immunocompetent patients due to the local containment of infection by the host response (6, 7).

Despite some recent progress in the development of novel antifungals, current treatment for cerebral cryptococcosis still uses drugs that were developed several decades ago (8, 9). The standard induction regimen combines the fungicidal polyene amphotericin B (AMB) with 5-fluorocytosine (10, 11). However, these drugs are not widely available and require intravenous administration and careful monitoring for drug-related toxicity. For these reasons, they are sometimes replaced by the oral drug fluconazole (FLC) in resource-limited settings, but monotherapy with this fungistatic drug is less efficacious (12). Despite recent advances in optimizing accessible combination therapies (13), the clinical need for effective, low-cost, and widely available anticryptococcal drugs with minimal toxicity remains high (14). Although new candidate drugs are frequently reported following *in vitro* screenings, only a very limited amount of these eventually reaches the clinic. For CNS infections, the presence of the blood-brain barrier (BBB) poses an additional hurdle in drug development. Even of the currently available antifungal compounds, only a few can efficiently reach the brain tissue (15).

To ensure an optimal translation from bench to bedside, testing the *in vivo* efficacy of a drug in animal models remains a crucial step as it allows studying the therapeutic response in a complex yet controlled system (16). Mammalian models allow the evaluation of therapy in the presence of an immune system and blood-brain barrier that is comparable to humans, including their potential disease-related changes. In murine models, response to antifungal treatment is frequently evaluated using survival curves, postmortem CFU analysis of the fungal load, or histopathologic examination of the isolated organs (16, 17). However, these techniques pose some challenges since they only provide single endpoint measurements of the disease status and limited information about spatial distribution of disease. When a temporal profile of drug efficacy is required, these studies rely on large groups of animals in order to isolate specific organs at predefined time points.

More recently, noninvasive imaging techniques have been developed that allow longitudinal evaluation of the fungal infection status or treatment response in individual animals. Bioluminescence imaging (BLI) measures the light emitted from the oxidation of a substrate by an enzyme such as *Gaussia* or firefly luciferase. Numerous studies have shown and extensively validated that the measured signal is proportional to the number of cells expressing the luciferase and their viability (18–23), since the intracellular ATP of living cells is essentially required for the light-emitting reaction of the firefly luciferase (24). By genetically engineering fungi to express this luciferase reporter gene, the *in vitro* activity of antifungal compounds (19, 23, 25) and the temporal and spatial distribution of the infectious burden in living animals can be monitored (23, 26–28). In this respect, treatment studies using animal models of aspergillosis and candidiasis have shown a good correlation between traditional CFU analysis of the fungal load and treatment effects observed in various organs by using BLI (19, 26, 27, 29). Previously, we have developed and validated the use of a novel bioluminescent *C. neoformans* strain for tracking pathogen dissemination from the lung to the brain (28). Thereby, we demonstrated a clear correlation between the number of CFU and the emitted light, both *in vitro* and *in vivo*. Furthermore, magnetic resonance imaging (MRI) of the brain allowed a detailed analysis of the spatial distribution of infectious foci. However, to date, preclinical imaging techniques have not been used to monitor antifungal treatment efficacy against fungal infections of the CNS, such as cryptococcosis.

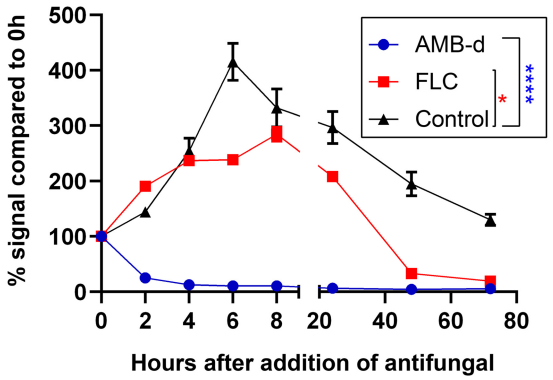

FIG 1 *In vitro* bioluminescence assay of antifungal effects. Amphotericin B deoxycholate (AMB-d; 0.1 mg/ml), fluconazole (FLC; 0.5 mg/ml), or sterile water (control) were added to pregrown (24-h-old) liquid cultures. Bioluminescence was measured immediately after, 2, 4, 6, 8, 24, 48, and 72 h after antifungal addition by adding D-luciferin (0.15 μg/ml) to samples of the culture. The bioluminescence signal is expressed relative to the signal obtained immediately after addition of antifungal (0 h). Curves were significantly different for AMB-d ($P < 0.0001$) and fluconazole ($P = 0.0152$) compared to the control curve. Two-way repeated measures ANOVA with Dunnett's multiple comparison posttest. The graph shows means ± the standard deviations (SD).

In this study, we assessed the use of BLI for screening the *in vitro* efficacy of antifungal compounds against *C. neoformans*. Second, we evaluated the combination of whole-body BLI and brain MRI to noninvasively monitor *in vivo* antifungal treatment efficacy with temporal and spatial resolution and validated this against standard CFU endpoint measurements. To this end, we tested liposomal AMB (L-AMB) or FLC monotherapy in murine models reflecting two distinct presentations of cerebral cryptococcosis: (i) a standard model of cryptococcal meningoencephalitis following disseminated disease and (ii) a model of a local cryptococcoma. In both cases, the treatment was delayed until BLI revealed that established disease was present. This late initiation of therapy was applied since it is similar to the clinical setting in which patients often present with advanced infection before being diagnosed. By obtaining longitudinal information on the dynamic process of treatment response in individual animals, we aimed to demonstrate the potential, validity, and added value of using noninvasive imaging in preclinical drug testing for fungal brain infections.

RESULTS

***In vitro* bioluminescence assays enable rapid real-time assessment of fungicidal and fungistatic antifungal drug activity.** To validate the potential of BLI to follow-up antifungal effects on cryptococcal cells, the bioluminescence emitted by *C. neoformans* reporter cells was measured *in vitro* at several time points after addition of amphotericin B deoxycholate (AMB-d) and FLC (Fig. 1). The BLI signal intensity of the untreated cells highly increased in the beginning (0 to 6 h), followed by a stable signal measured at 8 and 24 h and a subsequent decline in aging cultures. After addition of AMB-d (0.1 mg/ml), bioluminescence decreased to background levels within 2 h, indicating a rapid fungicidal effect of this drug at the tested concentration. Upon addition of the fungistatic drug FLC (0.5 mg/ml), the emitted bioluminescence initially continuously increased, but stagnated after 4 h, followed by a decrease after 24 h.

AMB induces a transient increase in bioluminescence that is potentially mediated by enhanced permeability for D-luciferin. After confirming the ability to detect antifungal effects using bioluminescence, we characterized the temporal profile of the bioluminescence signal in response to a wide concentration range of antifungals using a similar *in vitro* setup. At 8 and 26 h after exposure, a dose-dependent decrease in bioluminescence was observed for all tested concentrations of AMB-d and L-AMB, corresponding to its fungicidal effect (Fig. 2A and B, Fig. S1). When using the fungistatic agent FLC, the bioluminescence increased more slowly in cells exposed to higher

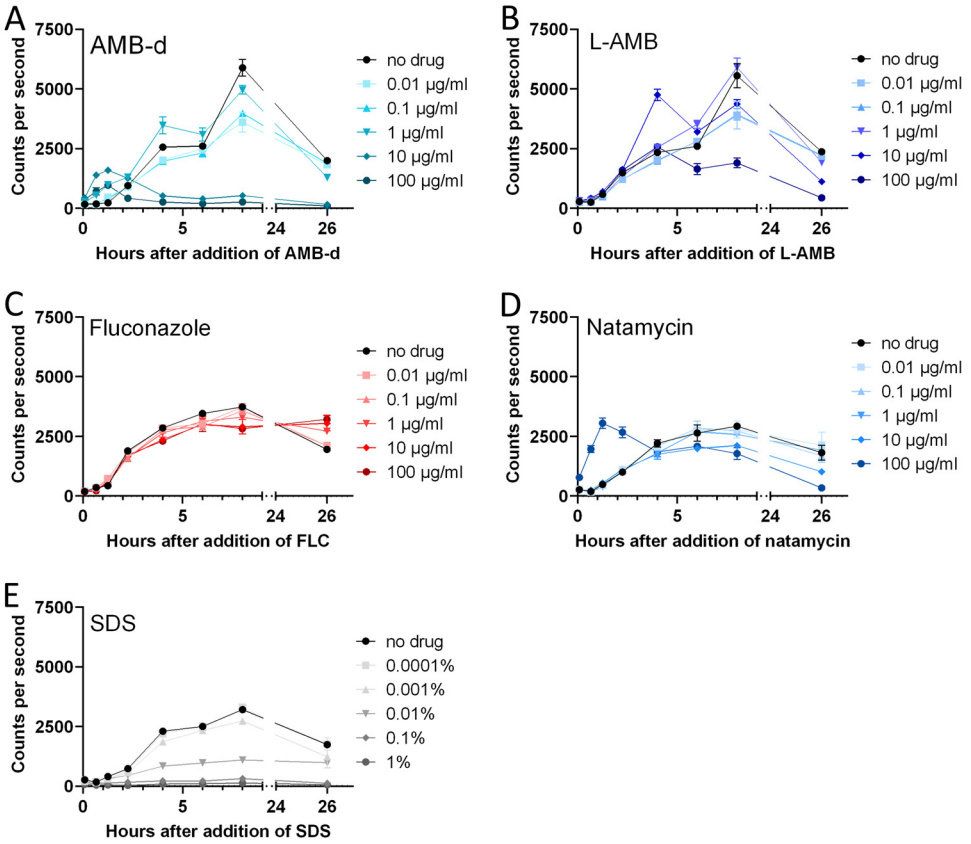

FIG 2 Temporal profile of the bioluminescence signals in response to different antifungal compounds. Bioluminescent *C. neoformans* cells in liquid culture (20 h old) were exposed to various doses of antifungals, and the bioluminescence was measured in real time at the indicated time points by adding D-luciferin to culture samples. (A) AMB-d showed a dose-dependent antifungal effect. Bioluminescence increased transiently shortly after addition. (B) L-AMB induced a similar but more delayed response. (C) Fluconazole showed a modest antifungal effect at the tested concentrations. (D) Exposure to natamycin induced a dose-dependent killing of the fungi. A transient increase was only observed for the highest concentration tested. (E) SDS caused a rapid dose-dependent decrease in bioluminescence. The graphs show means ± the SD.

concentrations (Fig. 2C; see also Fig. S1 in the supplemental material). At 8 h, we observed a dose-dependent reduction of bioluminescence compared to the control.

Bioluminescence transiently increased immediately after the addition of AMB-d or L-AMB, while a similar effect was not observed for FLC (Fig. 2; Fig. S1). Higher doses of AMB induced a larger and more rapid increase, which was smaller and more delayed for L-AMB compared to AMB-d.

We investigated potential explanations for this increased bioluminescence in parallel experiments, using a *C. neoformans* strain with a fluorescent E2-Crimson reporter gene under the control of the same promoter. Addition of the antifungals induced only a slight decrease in fluorescence, whereby the dose-dependent antifungal effect was most notable for FLC (Fig. S2). We did not observe increased fluorescence upon addition of the antifungals, indicating that a change in the expression levels of the reporter gene was not the cause of the increased bioluminescence. Furthermore, we found that none of the tested antifungals was autoluminescent or autofluorescent in water or Sabouraud medium (Fig. S3) nor caused luminescence in wild-type *C. neoformans* cells (Fig. S4).

Since AMB affects the integrity of the cell membrane and induces transmembrane channels (30, 31), we hypothesized that this transient bioluminescence increase might be caused by enhanced permeability of the fungal cells for the substrate D-luciferin (32). Exposure to natamycin, a polyene antifungal that does not permeabilize the plasma membrane (33), led to a dose-dependent decrease in bioluminescence corresponding to its

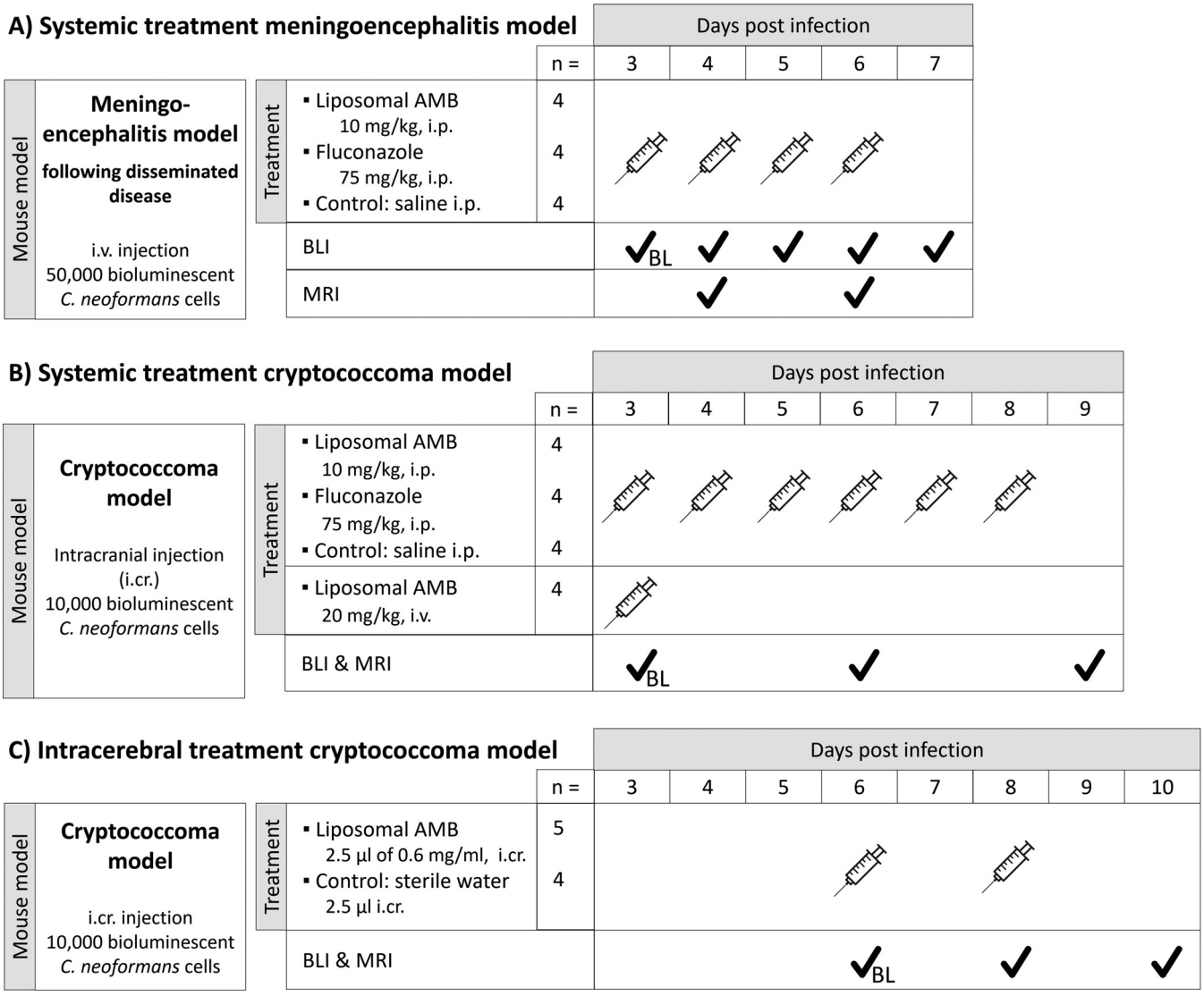

FIG 3 Experimental setups for *in vivo* imaging of treatment efficacy in delayed-treatment models. (A) Systemic treatment in the model of meningoencephalitis following disseminated disease. (B) Systemic treatment in the cryptococcoma model. (C) Intracerebral treatment in the cryptococcoma model. Abbreviations: i.cr., intracranial; i.p., intraperitoneal; i.v., intravenous; BL, baseline scans to assess infection status prior to initiation of treatment.

antifungal effect (Fig. 2D; Fig. S1). Only at the highest concentration tested (100 μg/ml), we observed a transient increase prior to this decrease. Exposure to sodium dodecyl sulfate (SDS), a surfactant leading to destruction of cell integrity and cell death, induced a rapid and dose-dependent reduction of bioluminescence (Fig. 2E; Fig. S1).

Whole-body BLI allows simultaneous evaluation of drug efficacy at multiple body sites in a model of disseminated cryptococcosis. We subsequently validated the use of BLI and MRI for *in vivo* evaluation of antifungal treatment efficacy by using different treatment regimens in a standard model of advanced cryptococcal meningoencephalitis following disseminated disease (Fig. 3A). After intravenous (i.v.) injection of cryptococci, control animals developed a progressive infection in the brain and the abdomen, including the spleen and kidney region, as previously described (28) (Fig. 4). The baseline infection status was assessed on day 3 and this identified an unsuccessful induction of infection in one animal of the FLC-treated group. Treatment with L-AMB significantly reduced the infection in the abdomen, while the bioluminescence from the brain was comparable to the control group. We observed a higher brain and abdomen bioluminescence in L-AMB treated animals than control animals specifically on day 4

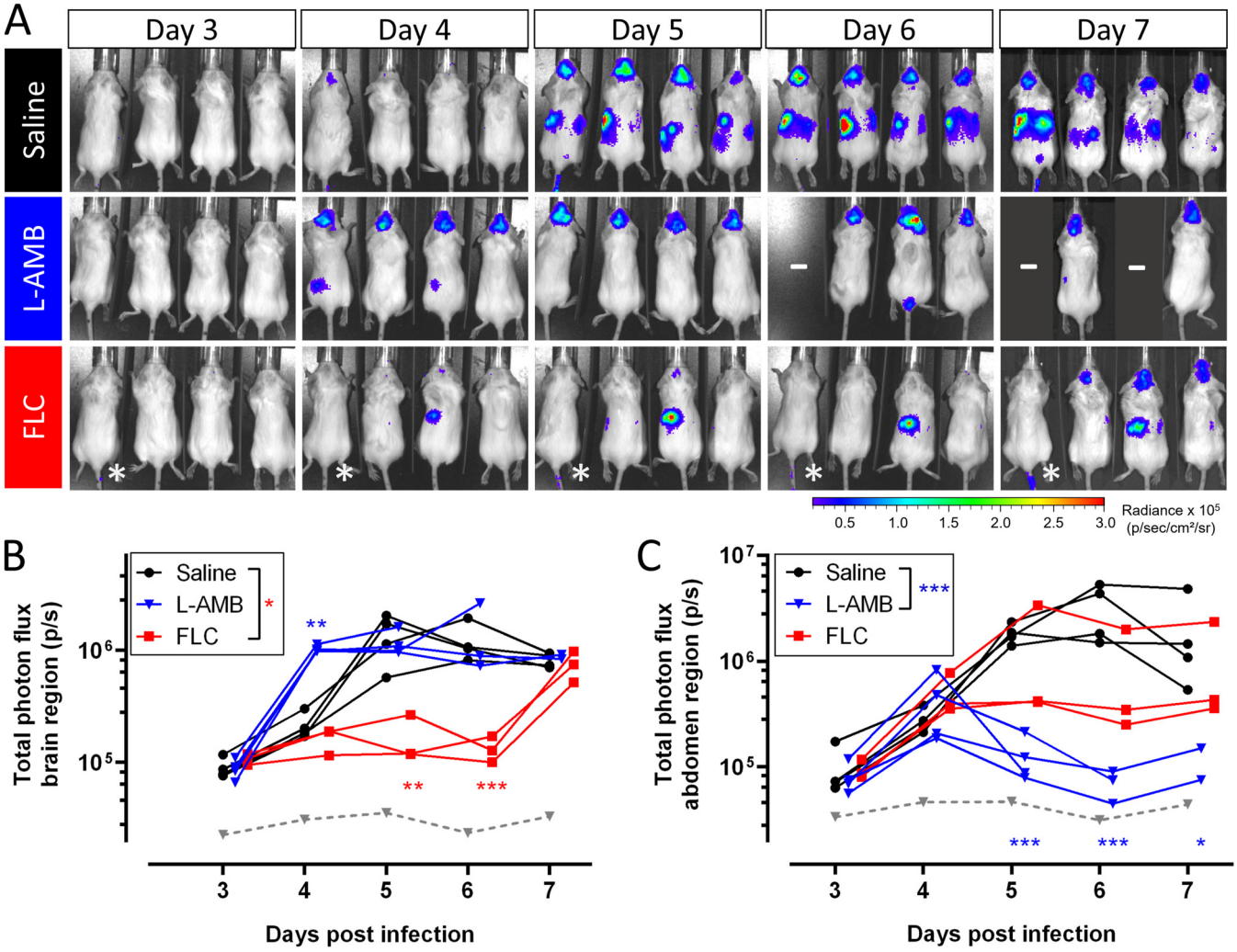

FIG 4 BLI of antifungal treatment efficacy in a model of cryptococcal meningoencephalitis. Animals ($n = 4$ per group) were i.v. injected with 50,000 bioluminescent *C. neoformans* cells and received daily injections with saline, L-AMB (10 mg/kg), or FLC (75 mg/kg) starting from day 3 p.i. One animal in the FLC group did not have an established infection and was excluded from further analysis (indicated by an asterisk [*] on the images and by a gray dashed line on the graphs). (A) BLI for the individual animals. (B) Quantification of the total photon flux in the brain region. The curves for FLC-treated animals were significantly different from the saline group ($P = 0.016$) but not for L-AMB-treated animals ($P = 0.7376$). On day 4, animals were injected with L-AMB shortly before BLI acquisition, leading to a significantly increased bioluminescence. (C) The total photon flux in the abdominal region was significantly lower in the L-AMB group than in the saline group ($P = 0.0001$) but not in the FLC group ($P = 0.4374$). Graphs show individual data points, assessed using mixed-effect model statistics with Dunnett's posttest. A minus sign (–) indicates that animals were lost to follow-up.

postinfection (p.i.), when imaging was performed less than 3 h after injection of antifungals. Animals treated with FLC showed a significant delay in the development of high brain signal intensity until day 6 p.i., after which the signal increased. The bioluminescence from the abdominal region was reduced compared to the control group, except for one animal that presented with a persistent hot spot in all images.

MRI of the brain showed that disease progression is associated with an increase in the total lesion volume, number of brain lesions and average volume per lesion (Fig. 5). L-AMB treatment induced a small reduction in the total lesion volume, but not in the number of brain lesions or their average volume. The MRI on day 4 p.i. did not show a difference between the L-AMB-treated and control animals that could explain the higher BLI signal intensity observed for the former group. Animals treated with FLC presented with a significantly lower total lesion volume and a smaller average lesion volume compared to untreated or L-AMB-treated animals. This was confirmed in lesion volume distributions obtained on day 6 (Fig. S5).

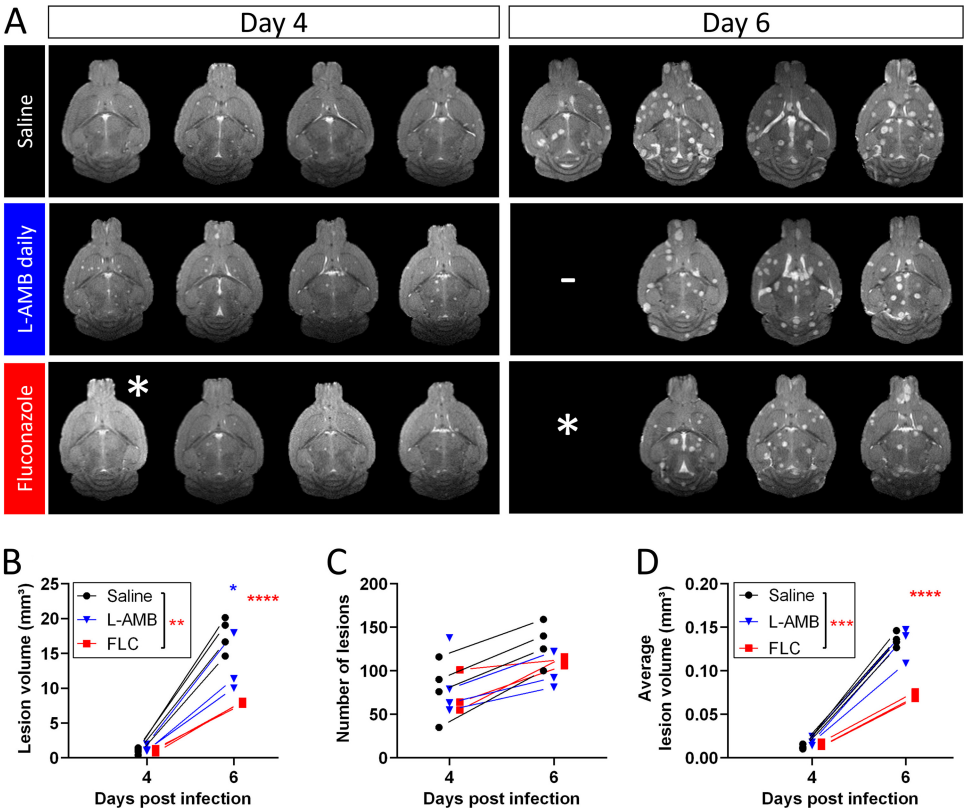

FIG 5 Brain MRI after antifungal treatment in the meningoencephalitis model. Daily antifungal treatment with L-AMB (10 mg/kg), FLC (75 mg/kg), or saline ($n = 4$ each) was initiated 3 days after i.v. injection with 50,000 *C. neoformans* cells. (A) Slice of the 2D coronal MR images for the individual animals (1 slice/animal). (B) The total lesion volume quantified from 3D MR images showed a significant effect for FLC treatment ($P = 0.0066$) but not for L-AMB treatment ($P = 0.2095$). (C) Treatment did not have a significant effect ($P = 0.8561$) on the number of lesions. (D) The average lesion volume was significantly lower in FLC-treated animals ($P = 0.0007$) but not in animals receiving L-AMB treatment ($P = 0.9740$). Graphs show individual data points, assessed using mixed-effect model statistics with Dunnett's posttest. A minus sign (–) indicates animals lost to follow-up; an asterisk (*) indicates one animal with unsuccessful induction of infection.

In agreement with the imaging results, CFU analysis showed that L-AMB led to a large reduction of the fungal load in the spleen and kidneys, while having a limited effect in the brain (Fig. 6). In comparison, FLC led to a larger reduction of the brain fungal load but had a more limited effect in the spleen and kidney. Quantitative cross-correlation of imaging results and CFU counts indicated that BLI results of the abdomen correlated well with the fungal load in the spleen and kidneys (Fig. S6). In the brain, the lesion volume quantified from the three-dimensional (3D) MRI was highly correlated with the fungal load. On day 7 p.i., we could not detect a significant correlation between the BLI results and the brain fungal burden, mainly due to the limited differences in the BLI signal. Nevertheless, we found that the BLI results on day 6 were predictive for the fungal burden on day 7, as evidenced by their good correlation.

BLI and MRI provide highly complementary information about the individual response to systemic therapy in a cryptococcoma model. In a second proof-of-concept study, we tested the combination of *in vivo* BLI and MRI for monitoring treatment efficacy in a mouse model of a local cryptococcoma (Fig. 3B). At baseline (day 3), established cryptococcomas were present in the mouse brains, with detectable bioluminescence and hyperintense focal lesions on the MR images (Fig. 7). The brain BLI signal intensity of untreated animals progressively increased (Fig. 7A and C) and was paralleled by an increase in the lesion volume on MRI (Fig. 7B and D). A single i.v. high dose of L-AMB showed no obvious treatment success. In contrast, animals treated with FLC generally presented with lower bioluminescence signal intensities and smaller

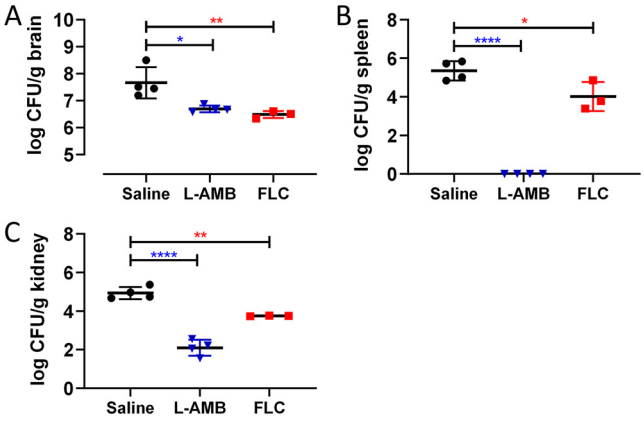

FIG 6 CFU analysis of the brain, spleen, and kidneys after antifungal treatment in the meningoencephalitis model. Disseminated infection was induced by i.v. injection of 50,000 *C. neoformans* cells. Fungal load analysis was performed after the last imaging session or when animals were sacrificed for humane endpoints. (A) L-AMB and FLC treatment induced a small reduction in the fungal load in the brain ($P = 0.0103$ and $P = 0.0054$, respectively). (B) FLC treatment reduced the fungal load in the spleen ($P = 0.0128$), while for L-AMB no fungal cells could be recovered ($P < 0.0001$). (C) L-AMB and FLC treatment lowered the fungal load in the kidneys ($P < 0.0001$ and $P = 0.0023$, respectively). Graphs show the means ± the SD, evaluated using one-way ANOVA with Dunnett's posttest.

brain lesions, indicating a response to antifungal therapy. Daily intraperitoneal (i.p.) injections with L-AMB led to large interanimal variability in the response. The animal with the smallest lesion at baseline showed low bioluminescence and limited lesion growth on MRI. One animal showed a limited increase in bioluminescence, while the lesion volume increased substantially. The other two animals presented with a large increase in BLI signal, but this was not associated with larger brain lesions on MRI. However, MRI indicated that the infection was no longer confined to the induced lesion and had spread into the ventricle or toward the front of the brain. The same was observed for one animal in the FLC-treated group. Histology confirmed that this presentation of the disease on MRI is typically associated with the presence of cryptococci in the ventricles (Fig. S7).

After the last imaging session on day 9, CFU analysis showed an approximate 10-fold reduction in the brain fungal load of most animals receiving daily L-AMB or FLC, although this difference was not significant (Fig. 8A). Invasion of the lesion into the ventricle was not associated with a higher fungal burden, except for one animal where infection had also spread to the front of the brain. The *in vivo* BLI results correlated well with the fungal burden in the brain (Fig. 8B), and exclusion of the few animals with ventricular involvement further strengthened this correlation. Furthermore, we found good correspondence between fungal burden and lesion volume on MRI (Fig. 8C).

Intracerebral amphotericin B treatment shows limited efficacy in the cryptococcoma model. Due to the limited antifungal effect observed in the cryptococcoma model upon systemic treatment with L-AMB, we subsequently evaluated the efficacy of direct intracerebral injection delivering L-AMB in the cryptococcoma, as this would bypass the role of the blood-brain barrier (BBB) in drug delivery (Fig. 3C). Similar to the control group, the brain BLI signal intensity increased for most animals in the L-AMB group, except for animal 1 and 2 that showed a stagnated BLI signal on day 10 (Fig. 9A and C). In contrast, the lesion volume increased for all animals (Fig. 9B and D). On some MR images, a small hyperintensity could be seen inside the lesion due to the injection. Its limited size compared to the whole lesion size could indicate that only part of the lesion was effectively targeted. CFU analysis showed a small but significant reduction in the fungal load, with limited variability within the group (Fig. S8). Although animals 1 and 2 showed a response on BLI, their fungal burdens and lesion volumes were similar to those of the other animals. This indicates that intracerebral injection of L-AMB in this cryptococcoma model is not superior to i.p. delivery of the drug.

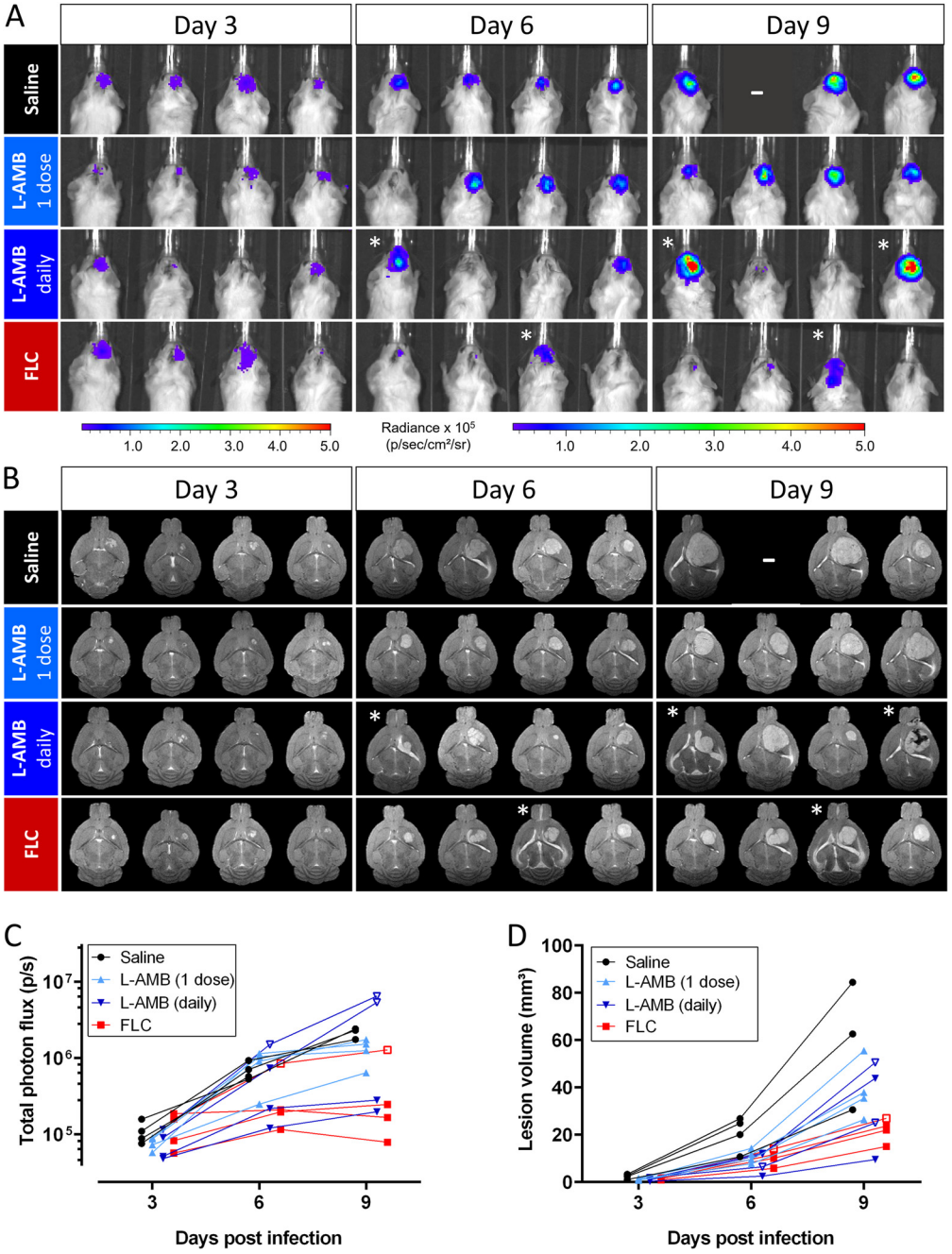

FIG 7 BLI and MRI of antifungal treatment efficacy following systemic treatment in the cryptococcoma model. Focal cryptococcomas were induced by stereotactic injection of 10,000 bioluminescent *C. neoformans* cells. Treatment ($n = 4$ per group) was initiated on day 3 by daily i.p. injection of FLC (75 mg/kg) or L-AMB (10 mg/kg), or a single i.v. dose (20 mg/kg) of L-AMB was given on day 3. (A) BLI of treated animals. (B) Coronal MRI slices for the corresponding animals (1 slice per animal). (C) Quantification of the BLI signal in the brain region. Statistics did not show an overall significant effect of treatment ($P = 0.2977$). (D) Lesion volume quantified from the MR images showed an overall significant effect of treatment ($P = 0.0354$) but no significant differences between the saline and treatment groups. Animals with higher bioluminescence and MRI-based evidence of cryptococcomas invading the ventricle are indicated by an asterisk (*) on the images and open symbols on the graphs. Graphs show individual data points, assessed using mixed-effect model statistics with Dunnett's posttest. A minus sign (–) indicates that animals were lost to follow-up.

DISCUSSION

Here, we have demonstrated that BLI enables qualitative and quantitative evaluation of the *in vitro* and *in vivo* therapeutic efficacy of antifungal compounds against *C. neoformans*. MRI provided a complementary readout on treatment effects by monitor-

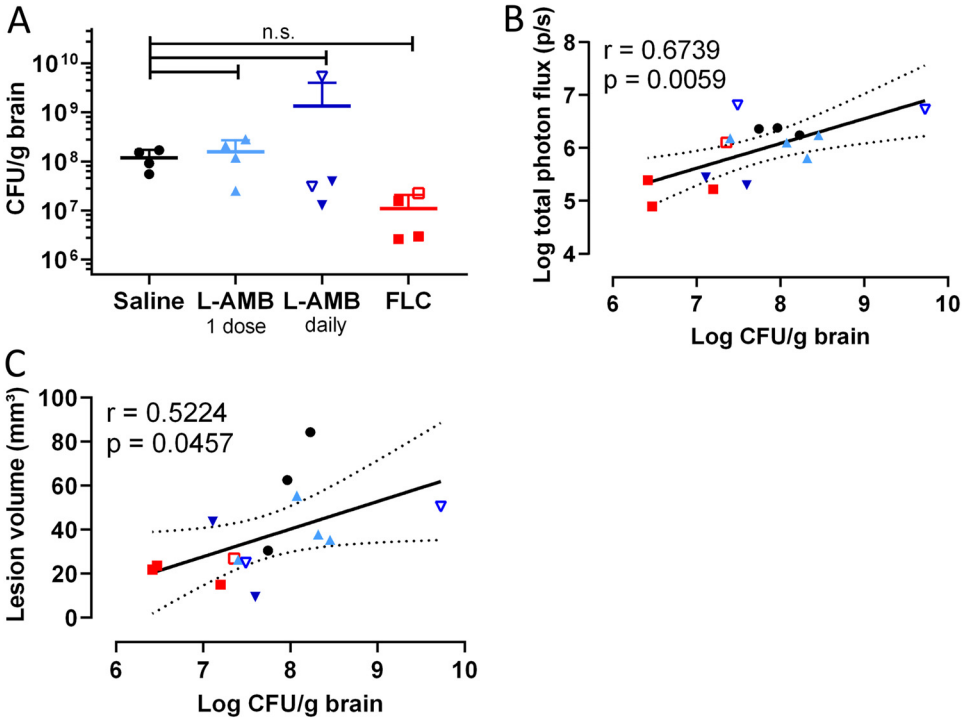

FIG 8 CFU analysis of the brains after systemic treatment in the cryptococcoma model and correlation with imaging readouts. (A) Treatment induced a small but not significant decrease in the fungal brain load in animals treated daily with FLC or L-AMB. No significant differences were found (overall *P* value = 0.0816). The animal with the notably higher brain fungal load in the L-AMB groups displayed spreading of the infection toward the front of the brain. (B and C) Quantification of *in vivo* BLI (B) and lesion volume obtained from MRI (C) correlated well with the fungal burden in the brain. When animals with spreading of the cryptococcomas to the ventricles (open symbols; also see Fig. 7) were excluded, the correlation of BLI and CFU results was strengthened ($r = 0.7491$, $P = 0.0050$). Graphs show data from individual animals. One-way ANOVA was performed with Dunnett's posttest or Pearson correlation coefficients with linear regression and 95% confidence bands.

ing the spatial distribution and growth rate of lesions in the brain. Both BLI and MRI results were in good agreement with CFU analysis, allowing a noninvasive *in vivo* assessment of the fungal load. In contrast to single time point measurements such as CFU analysis or histology, this novel approach provides information about the temporal and spatial evolution of the infection and therapeutic response in living animals and allows studying multiple infections sites simultaneously. Moreover, longitudinal imaging is noninvasive and reduces the number of animals needed for the preclinical evaluation of antifungal therapy as individual animals can be monitored throughout the full disease and treatment process. Therefore, the implementation of preclinical imaging can raise the ethical acceptance of *in vivo* efficacy studies, which remain an essential step for the evaluation of novel therapeutic compounds.

BLI enabled rapid real-time screening of *in vitro* antifungal drug efficacy with distinction between fungistatic and fungicidal activity. The use of real-time imaging techniques for determination of drug sensitivity and time-kill curves has the advantage that plating of samples for CFU counting can be neglected and results are obtained immediately (34). This makes BLI an interesting alternative for rapid real-time *in vitro* assessment of antifungal activity, and multiplexing BLI with fluorescence or dye-based approaches can provide additional validation of the results (19, 34). As some drugs induced a temporal increase in bioluminescence, robust testing of the antifungal effect should be done a broader time window to avoid measuring only these difficult to interpret transient effects. Alterations in membrane permeability causing an increased substrate influx are a possible contributor, and previous studies have used luciferase reporters to assess cell permeabilization in bacteria (32). Further study is warranted to investigate how this transient increase relates to the complex mode of action of

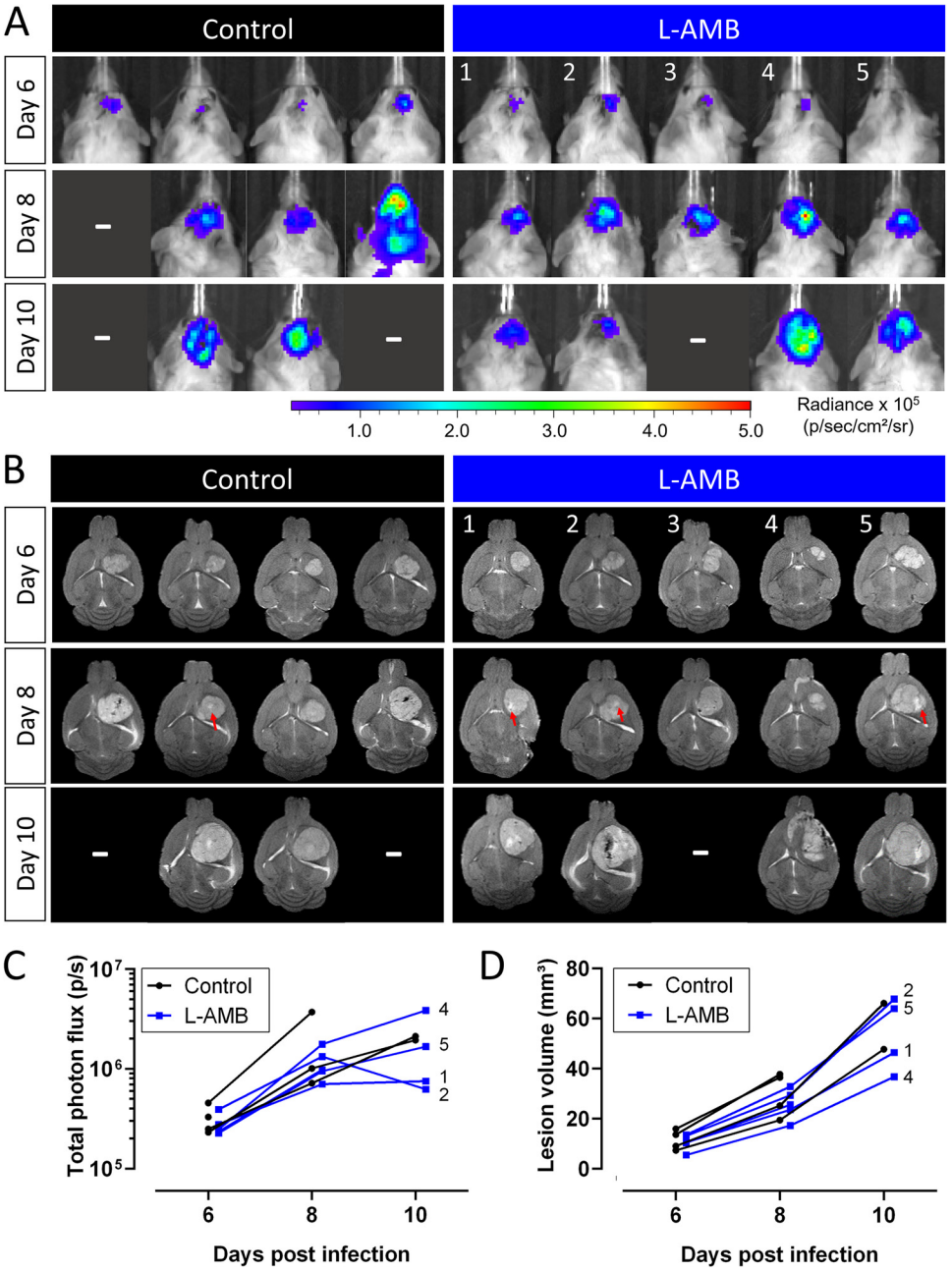

FIG 9 BLI and MRI of intracerebral treatment of cryptococcomas. Animals were stereotactically injected with 10,000 *C. neoformans* cells and L-AMB ($n = 5$) or sterile water ($n = 4$) was injected inside the brain lesion on days 6 and 8 p.i. (A) BLI of the infected animals on days 6 (before treatment), 8, and 10 p.i. (B) Slice of the coronal 2D brain MRI for the same animals, showing a small hyperintense region in the lesion at the site of injection (red arrows). (C) Quantification of the bioluminescence from the brain. (D) Quantification of the lesion volume on MRI. No significant effect of the treatment was found for the BLI or MRI results at group level ($P = 0.2725$ and $P = 0.4396$, respectively). Numbers on the graphs correspond to the specific animals on the images. Graphs show individual data points, assessed using mixed-effect model statistics with Dunnett's posttest. A minus sign (–) indicates that animals were lost to follow-up.

antifungals, and whether similar effects are also present with other bioluminescent organisms.

Subsequently, we aimed to validate a combination of noninvasive optical and anatomical imaging for *in vivo* evaluation of antifungal treatment efficacy in two mouse models and compared these to standard endpoint measurements such as CFU counts to quantify fungal load. Both BLI and MRI readouts correlated well with the fungal

burden in various organs, indicating that our dual imaging approach represents a valuable noninvasive alternative, or at least a compatible addition, to the traditional postmortem techniques. Even more so, our findings indicated that results from endpoint analyses can lead to misinterpretation of treatment effects and showed that these limitations can be overcome using noninvasive imaging. In the disseminated disease model, the therapeutic response was variable throughout the disease period, indicating that the selection of specific time points for fungal load analysis and correct identification of infected body sites (such as brain versus kidney infection) can have a large impact on conclusions about *in vivo* drug efficacy. Furthermore, our approach qualitatively and quantitatively assessed the infection status of individual animals prior to the start of treatment and identified animals in which induction of infection had failed, which might be wrongly interpreted as treatment success in single time point analyses. In addition, whole-body BLI allowed simultaneous assessment of the antifungal efficacy in various organs, including organs that were not in primary focus of this study. This contrasts techniques like CFU counting or histology, where effects are only studied in predefined organs. Hence, the implementation of this dual imaging approach in preclinical drug efficacy testing for CNS infections allows a more efficient and more complete assessment of the therapeutic effect than the standard techniques.

Overall, our BLI readouts correlated well to the current gold standard of CFU analysis, but for correct interpretation of BLI results it remains important to realize that several confounding factors may limit a direct translation from BLI signal to viable fungal load. First, the localization of infection affects the amount of detectable light. The BLI signal was higher when infection had spread to the ventricles and CSF compared to deep-seated, localized cryptococcomas, although this was not associated with an increased fungal load. Second, the bioluminescence reaction using firefly luciferases requires the availability of D-luciferin and the cofactors O_2, ATP, and Mg^{2+}. Especially in larger or necrotic lesions, the delivery of oxygen and the substrate D-luciferin might be limited, leading to a lower signal intensity (22). Changes in the BBB integrity could also affect the permeability for D-luciferin (35). Finally, we showed that some drugs may cause a transient BLI increase potentially due to altered membrane permeability and luciferin uptake, which could result in reduced correlation of the BLI signal with CFU counts. Our study illustrated that performing *in vivo* experiments in this specific time window of transient effects may lead to a transiently increased bioluminescence that is not necessarily related to an increased fungal load.

The addition of MRI provided a valuable second readout on treatment efficacy by monitoring with high spatial detail how antifungal treatment affects the growth rate and spatial distribution of brain lesions and limits damage to the host brain. In the meningoencephalitis model, MRI allowed the detailed analysis of the number of brain lesions and their respective sizes and showed an excellent correlation with the fungal load in the brain. Although MRI was able to demonstrate a slower growth rate of lesions upon treatment, successful antifungal therapy will most likely not result in rapid shrinkage of the lesion, as has also been shown in clinical MR studies (36). Since the hyperintense contrast on MRI is not specifically generated by viable fungi, the result of antifungal treatment will likely show a delayed response on MRI, in contrast to BLI, where a direct effect on fungal cell viability can be observed. However, in contrast to BLI, MRI does not require genetic modification of the fungal strain and is also implemented in a clinical setting.

The highly complementary information obtained by the combination of BLI and MRI can overcome the limitations of the individual imaging techniques. Our study showed that this is extremely valuable for correct interpretation of results. The acquired whole-body BLI images can be used to monitor and quantify the differential spatial and temporal distribution of infection and treatment effects in multiple organs simultaneously. BLI can guide additional anatomical imaging techniques toward organs of interest to obtain a detailed 3D localization of the infectious foci. MRI can provide an alternative readout on the infection status to validate the BLI results and identify potential reasons for specific observations with BLI. As an example, MRI showed the

spatial distribution of infection toward the ventricles or can detect bleeding or scar tissue which may attenuate the emitted light. In this way, BLI and MRI provide highly complementary information on different aspects of the therapeutic response: the direct effect on viable fungal load (BLI) or on lesion growth and damage to the host (MRI).

We have validated this novel imaging approach in two different animal models of cryptococcosis that represent two distinct clinical presentations of the disease. Treatment was generally less effective in the cryptococcoma model than the meningoencephalitis model, most likely due to limited drug penetration in large lesions. This corresponds to clinical case reports, where cryptococcomas are typically difficult to treat and require prolonged antifungal treatment and sometimes surgical resection (10, 37, 38). Moreover, meningoencephalitis models have a demonstrated impairment of the BBB integrity leading to more efficient penetration of AMB (39, 40), while this has not yet been investigated in cryptococcoma models. Preclinical studies using this model could help to optimize clinical treatment strategies for cryptococcomas.

Our present study validated the use of *in vivo* imaging techniques for noninvasive testing of treatment efficacy in various organs. It was not a direct aim of this proof-of-concept study to identify the most optimal treatment regimens for cryptococcosis. Accordingly, our study was sufficiently powered to demonstrate visually observable treatment effects with statistical validity, but a larger number of animals would likely be required for detecting potential more subtle effects. Our results indicated that the applied monotherapy regimens were insufficient to effectively clear the infection from all body sites. One reason for this limited efficacy of treatment can be attributed to the late start of therapy, which was initiated when disease had already been manifested. Such a limited efficacy of antifungal treatment has also been reported in other models with delayed treatment (26, 41) and underlines the importance of early diagnosis and rapid initiation of therapy (42, 43). Nonetheless, our results showed that *in vivo* antifungal efficacy in various organs can largely be attributed to the known biodistribution of the tested compounds. In the disseminated disease model, the potent fungicidal drug L-AMB reduced the infection load in the kidney and eradicated all cryptococci from the spleen, which is consistent with its high tissue concentration in this organ (44, 45). This was in contrast to the brain, where the best results were obtained using FLC, a drug that effectively crosses the BBB. Intraperitoneal injection with L-AMB only mildly reduced brain fungal load, consistent with its low availability in the brain which may hamper efficient control of CNS infections (15, 45). A higher treatment efficacy in the brain could potentially be achieved by i.v. injection of L-AMB through increased systemic uptake, although daily i.v. injections in mice are technically more challenging. An earlier initiation, prolonged treatment or combination therapy with different antifungals would likely also enhance treatment efficacy, and many different combinations and regimens have previously been evaluated in animal studies and clinical trials. Our proof-of-concept study shows that preclinical imaging is sensitive enough to detect even small treatment effects. As such, this work can form the basis for additional follow-up studies that search the most effective treatment strategy by use of preclinical imaging in appropriately powered animal studies.

In conclusion, we have shown that BLI and MRI allow noninvasive evaluation of the *in vivo* efficacy of antifungal compounds combatting CNS cryptococcosis. Both *in vitro* and *in vivo* BLI allowed for the rapid real-time assessment of the viable fungal load and its response to therapy, while treatment effects in multiple organs could be evaluated simultaneously. MRI allowed monitoring of the spatial distribution and growth rate of the brain lesions following antifungal treatment. The combination of both techniques provided highly complementary information and allowed longitudinal monitoring of the treatment effects in individual animals. This approach proved to be a powerful tool that can reveal important aspects of the dynamics of treatment response, which could be missed by single time point measurements like CFU and/or survival analyses and potentially lead to misinterpretation of therapeutic drug efficacy. Therefore, noninvasive *in vivo* imaging techniques have the potential to help improve the efficiency and

accuracy of preclinical drug testing for CNS infections and accelerate the translation of promising drug candidates or treatment regimens to the clinic.

MATERIALS AND METHODS

Fungal strains. The bioluminescent *C. neoformans* KN99α strain (28) expressing a red-shifted, codon-optimized firefly luciferase was used for both *in vitro* and *in vivo* experiments. Additional *in vitro* experiments were performed using a wild-type and red fluorescent *C. neoformans* KN99α strain, expressing the protein E2-Crimson (see the supplemental material for the construction of this strain). A green fluorescent protein (GFP)-expressing *C. neoformans* H99 strain (46) was used for histology of the infected brains. All *Cryptococcus* strains were cultured on Sabouraud agar (Bio-Rad, Temse, Belgium) for 2 to 3 days at 37°C (*in vitro*) or 30°C (*in vivo* experiments) prior to transfer to liquid cultures.

***In vitro* experiments. (i) Bioluminescence assay of antifungal effects.** Liquid cultures were grown in DYP medium (1% glucose, 0.5% yeast extract, 1% peptone) for 24 h at 37°C while shaking (200 rpm). Amphotericin B deoxycholate (AMB-d; 0.1 mg/ml; Fungizone; Bristol-Myers Squibb, Utrecht, The Netherlands), fluconazole (FLC; 0.5 mg/ml; TCI Europe, Zwijndrecht, Belgium), or an equal volume of sterile water (control) was added to the culture. Both drugs were dissolved or dispersed in sterile water. Cultures (10 ml) were incubated at 37°C while shaking, and samples were measured immediately after, 2, 4, 6, 8, 24, 48, and 72 h after addition of the antifungals. The results are expressed relative to the average signal obtained immediately after addition of the drug to normalize for differences in initial culture density.

(ii) Temporal profile of bioluminescence after antifungal therapy. Cultures were inoculated in liquid Sabouraud medium (Bio-Rad) and grown for 20 h at 37°C while shaking. AMB-d, liposomal amphotericin B (L-AMB; AmbiSome, Gilead Sciences, Carrigtohill, Ireland), FLC, natamycin (JK Scientific GmbH, Pforzheim, Germany), or SDS (Merck, Hohenbrunn, Germany) were dissolved or suspended in sterile water. Antifungal compounds were added to aliquots (4 ml) of the cultures at a final concentration of 0.01, 0.1, 1, 10, or 100 μg/ml, while SDS was used at 1, 0.1, 0.01, 0.001, and 0.0001%. An equal volume of sterile water was added to the no-drug control. Bioluminescence was measured at 5 min, 40 min, and 1, 2, 4, 6, 8, and 26 h after antifungal addition.

(iii) *In vitro* bioluminescence and fluorescence measurements. A 100-μl portion of the culture was transferred to a 96-well plate (Falcon Microtest 96; Becton Dickinson, Meylan, France) and 100 μl of D-luciferin (final concentration 0.15 μg/ml, in phosphate-buffered saline [PBS], Luciferin-EF; Promega) was added. Bioluminescence was measured in triplicate or quadruplicate samples using a plate reader (Wallac Victor 1420; PerkinElmer, Waltham, MA) with a 10-s measurement time. For assessment of fluorescent E2-Crimson strains, autofluorescence and autoluminescence, see the supplemental material.

***In vivo* experiments.** Animals were housed in individually ventilated cages and received water and standard food *ad libitum*. Female BALB/c mice (internal stock KU Leuven or Charles River Laboratories) were infected at an age of 9 to 10 weeks. All animal experiments were conducted in accordance with European directive 2010/63/EU and approved by the animal ethics committee of KU Leuven (P006/2017 and P103/2012).

(i) Preparation of *C. neoformans* inoculum. The bioluminescent *C. neoformans* strain was cultured in liquid Sabouraud medium for 2 to 3 days at 30°C. As previously described (28), fungal cells were harvested by centrifugation, washed twice with Dulbecco PBS (Gibco, Paisley, UK), counted using a Neubauer counting chamber and diluted to the desired concentration in PBS. The number of CFU in the inoculum was confirmed by plating on Sabouraud agar.

(ii) Experiment 1: systemic treatment in a meningoencephalitis model. For experiment 1, we utilized systemic treatment in a meningoencephalitis model (Fig. 3A). Animals were anaesthetized using 1.5 to 2% isoflurane (IsoVET; Primal Critical Care, Ltd., West Drayton, UK) in 100% oxygen and infected by tail vein injection of 50,000 fungal cells in 100 μl of PBS to induce disseminated infection and subsequent meningoencephalitis (28). Starting from day 3 p.i., animals ($n = 4$ per group) received antifungal treatment by i.p. injection of L-AMB (10 mg/kg), saline, or FLC (75 mg/kg). For the latter, we initially aimed to administer 150 mg/kg (corresponding to 800 mg/day in humans) based on previous reports of high-dose FLC treatment (47), but we found that this was not feasible due to the limited solubility of FLC in saline. L-AMB was dispersed in sterile water and diluted with 5% glucose solution prior to injection according to the manufacturer's instructions. One animal in the FLC group did not develop infection, most likely due to inefficient i.v. injection, and was excluded from the analysis. BLI scans were performed on days 3 (prior to antifungal treatment), 4, 5, 6, and 7, while 2D and 3D MRI scans were performed on days 4 and 6. BLI was performed prior to the daily dose of the antifungal, except on day 4.

(iii) Experiment 2: systemic treatment in a cryptococcoma model. For experiment 2, we utilized systemic treatment in a cryptococcoma model (Fig. 3B). Focal cryptococcal brain lesions were induced by intracranial stereotactic injection, based on a previously described rat model (48). Mice were anaesthetized by i.p. injection of ketamine (45 to 60 mg/kg; Nimatek; Eurovet Animal Health, Bladel, The Netherlands) and medetomidine (0.6 to 0.8 mg/kg; Domitor; Orion Pharma, Espoo, Finland). Fur on the head was clipped, the skin was disinfected, and local analgesia was administered (2% lidocaine; Linisol; Braun, Berlin, Germany). The animal's head was fixed in a stereotactic frame (Stoelting, Wood Dale, IL), and 10,000 bioluminescent *Cryptococcus* cells were injected (1 μl; rate, 0.5 μl/min) in the striatum using a 10-μl Hamilton syringe with a 30-gauge needle (Hamilton Company, Reno, NV). Injection coordinates were 0.5 mm anterior and 2 mm lateral to the bregma and 3 mm from the dura. To prevent backflow of the injected cells, the burr hole was closed using dental filling resin (NanoFil flowable light curing composite; AT&M Biomaterials, Beijing, China). The incision site was sutured, and anesthesia was reversed by i.p. injection of atipamezole hydrochloride (0.5 mg/kg; Antisedan; Orion Pharma). Additional animals

were injected with a GFP-expressing *C. neoformans* H99 strain for histological analysis of the cryptococcoma model (see the supplemental methods).

Starting from day 3 p.i., mice ($n = 4$ per group) received daily i.p. injections with saline, L-AMB (10 mg/kg), or FLC (75 mg/kg). A fourth group of animals received a single high dose of L-AMB (20 mg/kg) i.v., based on previous reports on the efficacy of this regimens (49). BLI and 2D MRI scans were performed on days 3 (prior to antifungal treatment), 6, and 9 p.i.

(iv) Experiment 3: intracerebral treatment in the cryptococcoma model. For experiment 3, we utilized intracerebral treatment in a cryptococcoma model (Fig. 3C). Focal cryptococcal brain lesions were induced by stereotactic injection. On days 6 and 8 p.i., mice ($n = 5$) received an intracranial stereotactic injection of L-AMB (2.5 μl of 0.6 mg/ml in sterile water) inside the brain lesion, at the same coordinates as used for induction. This volume (2.5 μl) was distributed in five steps of 0.5 μl, spaced every 0.5 mm between 4 and 2 mm from the dura. Control animals ($n = 4$) were injected with 2.5 μl of sterile water. Mice were scanned using BLI and MRI (2D) on days 6 (prior to the first treatment), 8, and 10.

Image acquisition and analysis. (i) BLI. Mice were injected i.p. with D-luciferin solution (15 mg/ml) at a dose of 126 mg/kg prior to anesthesia (50). Immediately afterward, animals were anaesthetized using 1.5 to 2% isoflurane in 100% oxygen. At 10 to 15 min after D-luciferin injection, mice were placed in prone position in an IVIS Spectrum imaging system (PerkinElmer) equipped with Living Image Software (version 4.5.2). Consecutive images were acquired during 30 min using an exposure time of 1 min, F/stop 1, subject height of 1.5 cm, and medium binning. The total photon flux was quantified using Living Image Software (version 4.5.4). Regions of interest were located in the brain (cryptococcoma model: circular ROI of 1.8-cm diameter; meningoencephalitis model: rectangular ROI of 1.6 by 1.3 cm) or upper abdomen (including spleen and kidney region, 2.5 by 1.3 cm). Per animal and time point, the highest total photon flux obtained from all consecutive images was used for further statistical analysis.

(ii) MRI. MR scans were acquired using a 9.4T preclinical MRI scanner with 20 cm bore (Biospec 94/20) and a linearly polarized resonator (72-mm diameter) in combination with an actively decoupled mouse brain surface coil (all Bruker Biospin, Ettlingen, Germany). A physiological monitoring system (Small Animal Instruments, Inc., Stony Brook, NY) was used to monitor each animal's breathing rate and body temperature during isoflurane anesthesia. After acquisition of localizer images, a 2D coronal T_2-weighted MR brain scan was acquired with the following parameters: spin-echo sequence; RARE factor of 8; TR/effective TE, 4,200/36.3 ms; field of view, 2 × 1.5 cm; 12 slices with 0.5-mm slice thickness; 100 μm in plane resolution; and a scan time of 1 min. A 2D axial brain scan was acquired with a RARE factor of 8, TR/effective TE of 4,200/36.3 ms, field of view of 2 × 2 cm, 9 slices with 0.5-mm thickness and a 0.2-mm slice gap, in-plane resolution of 78.125 μm, and a scan time of 1.66 min. The parameters for the 3D T_2-weighted brain MR scans (meningoencephalitis model) were as follows: spin-echo sequence, RARE factor 10, TR/TE 1,000/36 ms, FOV 2.4 × 1.5 × 0.83 cm, isotropic spatial resolution of approximately 94 μm, and a scan time of 15 min.

Lesions were manually delineated on the 2D or 3D scans using the brush tool in ITK-SNAP (version 3.4.0) (51). The reported lesion volume in the cryptococcoma model is the average volume obtained from the coronal and axial 2D scans. For the 3D scans in the meningoencephalitis model, the number of brain lesions and average volume per lesion was determined in ImageJ (version 1.49; National Institutes of Health, Bethesda, MD) (52) using the 3D object counter (53) after applying a Watershed algorithm on the segmentation image.

CFU analysis. After the last imaging session or when humane endpoints were reached, animals were sacrificed by i.p. injection of a pentobarbital overdose. The brains were isolated, weighed, and homogenized after the addition of PBS. Serial 10-fold dilutions were plated in triplicate on Sabouraud agar. After 3 days of incubation at room temperature or 2 days at 30°C, the number of colonies was counted manually. All reported CFU counts are expressed as CFU/g of tissue. For correlations with the imaging data, animals that succumbed to disease prior to the end of the experiments were excluded.

Statistical analysis. Data were analyzed using GraphPad Prism (version 8.1.2). Time-kill curves were analyzed using a two-way repeated-measures analysis of variance (ANOVA), followed by a Dunnett's posttest to compare each treatment group to the control curve. *In vitro* data at specific time points were analyzed using a one-way ANOVA with Dunnett's posttest compared to the control setting.

Longitudinal *in vivo* imaging data sets were analyzed using a mixed-effects model with Geisser-Greenhouse correction to investigate whether treatment effects were significant. If no significant effect was found, only this *P* value is reported. When treatment was a significant factor, *P* values for the comparison of specific treatment groups to the control group (over all time points) are reported after using a Dunnett's posttest. This was followed by a second Dunnett's posttest comparing the groups at the specific time points (significance indicated on the graph). CFU data were analyzed using an unpaired *t* test or one-way ANOVA with Dunnett's posttest and linear regression with Pearson correlation coefficients. *In vivo* BLI and CFU data were log transformed prior to statistical analysis.

SUPPLEMENTAL MATERIAL

Supplemental material is available online only.

SUPPLEMENTAL FILE 1, PDF file, 1.8 MB.

ACKNOWLEDGMENTS

We thank Jens Wouters and Sarah Belderbos for their assistance, and we thank Kristof Govaerts for his guidance with the MRI quantification. We gratefully acknowledge Steffen Fieuws (L-BioStat, KU Leuven) for statistical advice.

This study was funded by the European ERA-NET project CryptoView (third call of the FP7 program Infect-ERA), the Research Foundation-Flanders (FWO, 1506114N), and KU Leuven (PF 10/017 [IMIR], CREA/14/015). L.V. is a Ph.D. fellow strategic basic research at the FWO (151313). J.P. received a Ph.D. grant for strategic basic research from the Agency for Innovation by Science and Technology (IWT, 141230). G.V.V. received a postdoctoral fellowship from the FWO (12N7615N).

K.L. received consultancy fees from Pfizer, Abbott, MSD, and SMB Laboratoires Brussels and also received travel support from Pfizer and MSD and speaker fees from Gilead, MSD, Roche, Abbott (all outside the submitted work).

REFERENCES

1. Góralska K, Blaszkowska J, Dzikowiec M. 2018. Neuroinfections caused by fungi. Infection 46:443–459. https://doi.org/10.1007/s15010-018-1152-2.
2. Schwartz S, Kontoyiannis DP, Harrison T, Ruhnke M. 2018. Advances in the diagnosis and treatment of fungal infections of the CNS. Lancet Neurol 17:362–372. https://doi.org/10.1016/S1474-4422(18)30030-9.
3. Enoch DA, Yang H, Aliyu SH, Micallef C. 2017. The changing epidemiology of invasive fungal infections, p 17–65. *In* Lion T (ed), Human fungal pathogen identification. Methods in Molecular Biology, vol 1508. Humana Press, New York, NY. https://doi.org/10.1007/978-1-4939-6515-1_2.
4. Lee SC, Dickson DW, Casadevall A. 1996. Pathology of cryptococcal meningoencephalitis: analysis of 27 patients with pathogenetic implications. Hum Pathol 27:839–847. https://doi.org/10.1016/s0046-8177(96)90459-1.
5. Williamson PR, Jarvis JN, Panackal AA, Fisher MC, Molloy SF, Loyse A, Harrison TS. 2017. Cryptococcal meningitis: epidemiology, immunology, diagnosis, and therapy. Nat Rev Neurol 13:13–24. https://doi.org/10.1038/nrneurol.2016.167.
6. Chen S, Sorrell T, Nimmo G, Speed B, Currie B, Ellis D, Marriott D, Pfeiffer T, Parr D, Byth K. 2000. Epidemiology and host- and variety-dependent characteristics of infection due to *Cryptococcus neoformans* in Australia and New Zealand. Clin Infect Dis 31:499–508. https://doi.org/10.1086/313992.
7. Nguyen MH, Husain S, Clancy CJ, Peacock JE, Hung C-C, Kontoyiannis DP, Morris AJ, Heath CH, Wagener M, Yu VL. 2010. Outcomes of central nervous system cryptococcosis vary with host immune function: results from a multi-center, prospective study. J Infect 61:419–426. https://doi.org/10.1016/j.jinf.2010.08.004.
8. Roemer T, Krysan DJ. 2014. Antifungal drug development: challenges, unmet clinical needs, and new approaches. Cold Spring Harb Perspect Med 4:a019703–a019703. https://doi.org/10.1101/cshperspect.a019703.
9. Perfect JR. 2017. The antifungal pipeline: a reality check. Nat Rev Drug Discov 16:603–616. https://doi.org/10.1038/nrd.2017.46.
10. Sloan D, Parris V. 2014. Cryptococcal meningitis: epidemiology and therapeutic options. Clin Epidemiol 6:169–182. https://doi.org/10.2147/CLEP.S38850.
11. World Health Organization. 2018. Guidelines for the diagnosis, prevention, and management of cryptococcal disease in HIV-infected adults, adolescents, and children: supplement to the 2016 consolidated guidelines on the use of antiretroviral drugs for treating and preventing HIV infection. World Health Organization, Geneva, Switzerland.
12. Sloan DJ, Dedicoat MJ, Lalloo DG. 2009. Treatment of cryptococcal meningitis in resource limited settings. Curr Opin Infect Dis 22:455–463. https://doi.org/10.1097/QCO.0b013e32832fa214.
13. Molloy SF, ACTA Trial Study Team, Kanyama C, Heyderman RS, Loyse A, Kouanfack C, Chanda D, Mfinanga S, Temfack E, Lakhi S, Lesikari S, Chan AK, Stone N, Kalata N, Karunaharan N, Gaskell K, Peirse M, Ellis J, Chawinga C, Lontsi S, Ndong J-G, Bright P, Lupiya D, Chen T, Bradley J, Adams J, van der Horst C, van Oosterhout JJ, Sini V, Mapoure YN, Mwaba P, Bicanic T, Lalloo DG, Wang D, Hosseinipour MC, Lortholary O, Jaffar S, Harrison TS. 2018. Antifungal combinations for treatment of cryptococcal meningitis in Africa. N Engl J Med 378:1004–1017. https://doi.org/10.1056/NEJMoa1710922.
14. Krysan DJ. 2015. Toward improved anti-cryptococcal drugs: novel molecules and repurposed drugs. Fungal Genet Biol 78:93–98. https://doi.org/10.1016/j.fgb.2014.12.001.
15. Felton T, Troke PF, Hope WW. 2014. Tissue penetration of antifungal agents. Clin Microbiol Rev 27:68–88. https://doi.org/10.1128/CMR.00046-13.
16. Capilla J, Clemons KV, Stevens DA. 2007. Animal models: an important tool in mycology. Med Mycol 45:657–684. https://doi.org/10.1080/13693780701644140.
17. Hohl TM. 2014. Overview of vertebrate animal models of fungal infection. J Immunol Methods 410:100–112. https://doi.org/10.1016/j.jim.2014.03.022.
18. Avci P, Karimi M, Sadasivam M, Antunes-Melo WC, Carrasco E, Hamblin MR. 2018. *In-vivo* monitoring of infectious diseases in living animals using bioluminescence imaging. Virulence 9:28–63. https://doi.org/10.1080/21505594.2017.1371897.
19. Vande Velde G, Kucharíková S, Van Dijck P, Himmelreich U. 2018. Bioluminescence imaging increases *in vivo* screening efficiency for antifungal activity against device-associated *Candida albicans* biofilms. Int J Antimicrob Agents 52:42–51. https://doi.org/10.1016/j.ijantimicag.2018.03.007.
20. Persyn A, Rogiers O, Brock M, Vande Velde G, Lamkanfi M, Jacobsen ID, Himmelreich U, Lagrou K, Van Dijck P, Kucharíková S. 2018. Monitoring of fluconazole and caspofungin activity against *in vivo Candida glabrata* biofilms by bioluminescence imaging. Antimicrob Agents Chemother 63:e01555-18. https://doi.org/10.1128/AAC.01555-18.
21. Vande Velde G, Kucharíková S, Schrevens S, Himmelreich U, Van Dijck P. 2014. Towards noninvasive monitoring of pathogen-host interactions during *Candida albicans* biofilm formation using *in vivo* bioluminescence. Cell Microbiol 16:115–130. https://doi.org/10.1111/cmi.12184.
22. Brock M, Jouvion G, Droin-Bergère S, Dussurget O, Nicola M-A, Ibrahim-Granet O. 2008. Bioluminescent *Aspergillus fumigatus*, a new tool for drug efficiency testing and *in vivo* monitoring of invasive aspergillosis. Appl Environ Microbiol 74:7023–7035. https://doi.org/10.1128/AEM.01288-08.
23. Galiger C, Brock M, Jouvion G, Savers A, Parlato M, Ibrahim-Granet O. 2013. Assessment of efficacy of antifungals against *Aspergillus fumigatus*: value of real-time bioluminescence imaging. Antimicrob Agents Chemother 57:3046–3059. https://doi.org/10.1128/AAC.01660-12.
24. Kaskova ZM, Tsarkova AS, Yampolsky IV. 2016. 1001 lights: luciferins, luciferases, their mechanisms of action and applications in chemical analysis, biology, and medicine. Chem Soc Rev 45:6048–6077. https://doi.org/10.1039/C6CS00296J.
25. Binder U, Navarro-Mendoza MI, Naschberger V, Bauer I, Nicolas FE, Pallua JD, Lass-Flörl C, Garre V, Binder U, Navarro-Mendoza MI, Naschberger V, Bauer I, Nicolas FE, Pallua JD, Lass-Flörl C, Garre V. 2018. Generation of a *Mucor circinelloides* reporter strain: a promising new tool to study antifungal drug efficacy and mucormycosis. Genes (Basel) 9:613. https://doi.org/10.3390/genes9120613.
26. Poelmans J, Himmelreich U, Vanherp L, Zhai L, Hillen A, Holvoet B, Belderbos S, Brock M, Maertens J, Vande Velde G, Lagrou K. 2018. A multimodal imaging approach enables *in vivo* assessment of antifungal treatment in a mouse model of invasive pulmonary aspergillosis. Antimicrob Agents Chemother 62:e00240-18. https://doi.org/10.1128/AAC.00240-18.
27. Jacobsen ID, Lüttich A, Kurzai O, Hube B, Brock M. 2014. *In vivo* imaging of disseminated murine *Candida albicans* infection reveals unexpected host sites of fungal persistence during antifungal therapy. J Antimicrob Chemother 69:2785–2796. https://doi.org/10.1093/jac/dku198.
28. Vanherp L, Ristani A, Poelmans J, Hillen A, Lagrou K, Janbon G, Brock M, Himmelreich U, Vande Velde G. 2019. Sensitive bioluminescence imaging of fungal dissemination to the brain in mouse models of cryptococ-

cosis. Dis Model Mech 12:dmm039123. https://doi.org/10.1242/dmm.039123.
29. Dorsaz S, Coste AT, Sanglard D. 2017. Red-shifted firefly luciferase optimized for *Candida albicans in vivo* bioluminescence imaging. Front Microbiol 8:1478. https://doi.org/10.3389/fmicb.2017.01478.
30. Palacios DS, Dailey I, Siebert DM, Wilcock BC, Burke MD. 2011. Synthesis-enabled functional group deletions reveal key underpinnings of amphotericin B ion channel and antifungal activities. Proc Natl Acad Sci U S A 108:6733–6738. https://doi.org/10.1073/pnas.1015023108.
31. Bolard J. 1986. How do the polyene macrolide antibiotics affect the cellular membrane properties? Biochim Biophys Acta 864:257–304. https://doi.org/10.1016/0304-4157(86)90002-x.
32. Virta M, Åkerman KEO, Saviranta P, Oker-Blom C, Karp MT. 1995. Real-time measurement of cell permeabilization with low-molecular-weight membranolytic agents. J Antimicrob Chemother 36:303–315. https://doi.org/10.1093/jac/36.2.303.
33. Te Welscher YM, ten Napel HH, Balagué MM, Souza CM, Riezman H, de Kruijff B, Breukink E. 2008. Natamycin blocks fungal growth by binding specifically to ergosterol without permeabilizing the membrane. J Biol Chem 283:6393–6401. https://doi.org/10.1074/jbc.M707821200.
34. Van Dijck P, Sjollema J, Cammue BP, Lagrou K, Berman J, d'Enfert C, Andes DR, Arendrup MC, Brakhage AA, Calderone R, Cantón E, Coenye T, Cos P, Cowen LE, Edgerton M, Espinel-Ingroff A, Filler SG, Ghannoum M, Gow NAR, Haas H, Jabra-Rizk MA, Johnson EM, Lockhart SR, Lopez-Ribot JL, Maertens J, Munro CA, Nett JE, Nobile CJ, Pfaller MA, Ramage G, Sanglard D, Sanguinetti M, Spriet I, Verweij PE, Warris A, Wauters J, Yeaman MR, Zaat SAJ, Thevissen K. 2018. Methodologies for *in vitro* and *in vivo* evaluation of efficacy of antifungal and antibiofilm agents and surface coatings against fungal biofilms. Microb Cell 5:300–326. https://doi.org/10.15698/mic2018.07.638.
35. Ayzenberg I, Schlevogt S, Metzdorf J, Stahlke S, Pedreitturia X, Hunfeld A, Couillard-Despres S, Kleiter I. 2015. Analysis of neurogenesis during experimental autoimmune encephalomyelitis reveals pitfalls of bioluminescence imaging. PLoS One 10:e0118550. https://doi.org/10.1371/journal.pone.0118550.
36. Hospenthal DR, Bennett JE. 2000. Persistence of cryptococcomas on neuroimaging. Clin Infect Dis 31:1303–1306. https://doi.org/10.1086/317434.
37. Perfect JR, Dismukes WE, Dromer F, Goldman DL, Graybill JR, Hamill RJ, Harrison TS, Larsen RA, Lortholary O, Nguyen M-H, Pappas PG, Powderly WG, Singh N, Sobel JD, Sorrell TC. 2010. Clinical practice guidelines for the management of cryptococcal disease: 2010 update by the Infectious Diseases Society of America. Clin Infect Dis 50–322. https://doi.org/10.1086/649858.
38. Ulett KB, Cockburn JWJ, Jeffree R, Woods ML. 2017. Cerebral cryptococcoma mimicking glioblastoma. BMJ Case Rep 2017:bcr2016218824. https://doi.org/10.1136/bcr-2016-218824.
39. Pai MP, Sakoglu U, Peterson SL, Lyons CR, Sood R. 2009. Characterization of BBB permeability in a preclinical model of cryptococcal meningoencephalitis using magnetic resonance imaging. J Cereb Blood Flow Metab 29:545–553. https://doi.org/10.1038/jcbfm.2008.144.
40. Takemoto K, Yamamoto Y, Ueda Y. 2006. Influence of the progression of cryptococcal meningitis on brain penetration and efficacy of AmBisome in a murine model. Chemotherapy 52:271–278. https://doi.org/10.1159/000095820.
41. Lu R, Hollingsworth C, Qiu J, Wang A, Hughes E, Xin X, Konrath KM, Elsegeiny W, Park Y-D, Atakulu L, Craft JC, Tramont EC, Mannino R, Williamson PR. 2019. Efficacy of oral encochleated amphotericin B in a mouse model of cryptococcal meningoencephalitis. mBio 10:e00724-19. https://doi.org/10.1128/mBio.00724-19.
42. Pasquier E, Kunda J, De Beaudrap P, Loyse A, Temfack E, Molloy SF, Harrison TS, Lortholary O. 2018. Long-term mortality and disability in cryptococcal meningitis: a systematic literature review. Clin Infect Dis 66:1122–1132. https://doi.org/10.1093/cid/cix870.
43. Aye C, Henderson A, Yu H, Norton R. 2016. Cryptococcosis: the impact of delay to diagnosis. Clin Microbiol Infect 22:632–635. https://doi.org/10.1016/j.cmi.2016.04.022.
44. Bellmann R, Smuszkiewicz P. 2017. Pharmacokinetics of antifungal drugs: practical implications for optimized treatment of patients. Infection 45:737–779. https://doi.org/10.1007/s15010-017-1042-z.
45. Vogelsinger H, Weiler S, Djanani A, Kountchev J, Bellmann-Weiler R, Wiedermann CJ, Bellmann R. 2006. Amphotericin B tissue distribution in autopsy material after treatment with liposomal amphotericin B and amphotericin B colloidal dispersion. J Antimicrob Chemother 57:1153–1160. https://doi.org/10.1093/jac/dkl141.
46. Voelz K, Johnston SA, Rutherford JC, May RC. 2010. Automated analysis of cryptococcal macrophage parasitism using GFP-tagged cryptococci. PLoS One 5:e15968. https://doi.org/10.1371/journal.pone.0015968.
47. Santos JRA, Ribeiro NQ, Bastos RW, Holanda RA, Silva LC, Queiroz ER, Santos DA. 2017. High-dose fluconazole in combination with amphotericin B is more efficient than monotherapy in murine model of cryptococcosis. Sci Rep 7:4661. https://doi.org/10.1038/s41598-017-04588-7.
48. Himmelreich U, Dzendrowskyj TE, Allen C, Dowd S, Malik R, Shehan BP, Russell P, Mountford CE, Sorrell TC. 2001. Cryptococcomas distinguished from gliomas with MR spectroscopy: an experimental rat and cell culture study. Radiology 220:122–128. https://doi.org/10.1148/radiology.220.1.r01jl25122.
49. Lestner J, McEntee L, Johnson A, Livermore J, Whalley S, Schwartz J, Perfect JR, Harrison T, Hope W. 2017. Experimental models of short courses of liposomal amphotericin B for induction therapy for cryptococcal meningitis. Antimicrob Agents Chemother 61:e00090-17. https://doi.org/10.1128/AAC.00090-17.
50. Aswendt M, Adamczak J, Couillard-Despres S, Hoehn M, Bailly C, Gaensler K. 2013. Boosting bioluminescence neuroimaging: an optimized protocol for brain studies. PLoS One 8:e55662. https://doi.org/10.1371/journal.pone.0055662.
51. Yushkevich PA, Piven J, Hazlett HC, Smith RG, Ho S, Gee JC, Gerig G. 2006. User-guided 3D active contour segmentation of anatomical structures: significantly improved efficiency and reliability. Neuroimage 31:1116–1128. https://doi.org/10.1016/j.neuroimage.2006.01.015.
52. Schneider CA, Rasband WS, Eliceiri KW. 2012. NIH Image to ImageJ: 25 years of image analysis. Nat Methods 9:671–675. https://doi.org/10.1038/nmeth.2089.
53. Bolte S, Cordelières FP. 2006. A guided tour into subcellular colocalization analysis in light microscopy. J Microsc 224:213–232. https://doi.org/10.1111/j.1365-2818.2006.01706.x.